**D-2-Hydroxyglutarate dehydrogenase connects the propionate shunt to ketone body metabolism in *Caenorhabditis elegans***

Olga Ponomarova[1], Hefei Zhang[1], Xuhang Li[1], Shivani Nanda[1], Thomas B. Leland[1], Bennett W. Fox[2], Gabrielle E. Giese[1], Frank C. Schroeder[2], L. Safak Yilmaz[1], Albertha J.M. Walhout[1]

1 Department of Systems Biology, University of Massachusetts Chan Medical School, Worcester, MA, USA

2 Boyce Thompson Institute and Department of Chemistry and Chemical Biology, Cornell University, Ithaca, NY, USA

Email: marian.walhout@umassmed.edu

**D-2-hydroxyglutaric aciduria is a rare inborn error of human metabolism caused by loss-of-function mutations in D-2-hydroxyglutarate(D-2HG) dehydrogenase (D2HGDH) resulting in the accumulation of D-2HG[1]. D-2HG inhibits multiple metabolic enzymes[2-4] and promotes tumorigenesis[5,6], however the endogenous metabolism of D-2HG remains poorly understood. Here, we find that, in the nematode *Caenorhabditis elegans*, the propionate shunt enzyme HPHD-1[7] produces D-2HG in a reaction coupled to oxidation of 3-hydroxypropionate (3HP), and that the D-2HG dehydrogenase DHGD-1 recycles D-2HG to α–ketoglutarate (αKG). *dhgd-1* deletion mutants exhibit embryonic lethality, which can be rescued by vitamin B12 supplementation or by *hphd-1* RNAi. Remarkably, neither D-2HG nor 3HP accumulation in these mutants explains embryonic lethality. Instead, ketone body metabolism genes are upregulated and supplementation of the ketone body 3-hydroxybutyrate (3HB) partially rescues embryonic lethality. Altogether, our findings suggest that propionate and ketone bodies are functionally connected to support *C. elegans* viability.**

The metabolite 2HG occurs as two enantiomers, L-2HG and D-2HG, each of which is oxidized by a specific dehydrogenase. Mutations in these dehydrogenases result in L- and D-2-hydroxyglutaric aciduria, respectively[8,9]. These diseases cause the accumulation of 2HG in bodily fluids, delayed development, neurological dysfunction, and early death[10]. While the metabolism of L-2HG has been studied in model organisms such as *Drosophila*[11], the endogenous production and consumption of D-2HG, and the consequences of its accumulation, remain poorly understood.

We identified the *C. elegans* gene F54D5.12 as a one-to-one ortholog of human D2HGDH and named this gene *dhgd-1* for D-2-hydroxyglutarate dehydrogenase. We first asked whether DHGD-1 is indeed a D-2HG dehydrogenase that converts D-2HG into αKG (Fig. 1a). We obtained *dhgd-1(tm6671)* mutant animals that carry a large deletion in the 5' end of the gene, which is predicted to result in a loss-of-function (Fig. 1b). These animals are hereafter referred to as Δ*dhgd-1* mutants. By gas chromatography-mass spectrometry (GC-MS), we found that Δ*dhgd-1* mutants accumulate about five-

fold more 2HG than wild type animals (Fig. 1c). Human D2HGDH specifically catalyzes the conversion of the D-form of 2HG[12]. To test the stereo-specificity of *C. elegans* DHGD-1, we used chiral derivatization that allows the chromatographic separation of the D- and L-2HG enantiomers. While in wild type animals the ratio between L- and D-2HG is about one to one, Δ*dhgd-1* mutant animals predominantly accumulate the D-2HG enantiomer, confirming that DHGD-1 is indeed a functional ortholog of human D2HGDH (Fig. 1d). We found that Δ*dhgd-1* mutant animals have severe embryonic lethality as approximately two thirds of the embryos failed to hatch (Figs. 1e, f). In addition, Δ*dhgd-1* mutant animals exhibit mitochondrial defects as their mitochondrial network is more fragmented and individual mitochondria are more rounded, which is in agreement with recently reported data[13] (Extended Data Fig. 1a). These observations allow us to investigate the connection between organismal physiology and endogenous D-2HG metabolism.

The Δ*dhgd-1* mutant metabolome exhibits several additional changes in metabolite abundance: lower accumulation of glutamate, αKG, succinate, and the lysine breakdown products 2-aminoadipate and glutarate, as well as higher accumulation of lysine, β-alanine, and 3-aminoisobutyrate, and the leucine breakdown product 3,3-hydroxymethylbutyrate (HMB) (Fig. 2a). Importantly, 3HP, a metabolite unique to the propionate shunt[7], exhibited the greatest increase in abundance in Δ*dhgd-1* mutant animals, which suggests that loss of *dhgd-1* interferes with the function of the propionate shunt.

Interestingly, four of the five propionate shunt genes are strongly coexpressed with *dhgd-1* (Fig. 2b,c)(Extended Data Table 1). One of these, *hphd-1*, is an ortholog of human ADHFE1, which produces D-2HG in a reaction coupled to oxidation of the neurotransmitter and psychoactive drug γ-hydroxybutyrate[14]. Therefore, we hypothesized that HPHD-1 reduces αKG to D-2HG when it oxidizes 3HP to malonic semialdehyde[7], and that DHGD-1 recycles D-2HG back to αKG (Fig. 2d). Since HPHD-1 harbors a highly conserved Rossman fold that can bind nucleic acid cofactors such as NAD+, we predicted that HPHD-1 uses NAD+/NADH to shuttle a hydride from 3HP to D-2HG (Fig. 2e)[15]. If true, this leads to the prediction that D-2HG is derived from propionate degradation. To directly test this, we performed a stable isotope tracing experiment in which animals were supplemented with either

propionate or deuterated $^{2}H_5$-propionate. Supplementing $^{2}H_5$-propionate produced both deuterated 3HP and D-2HG, while the bacterial diet alone did not contain any detectable 3HP or 2HG, showing that these conversions happen in the animal (Fig. 2f, g, h, Extended Data Fig. 2). This result demonstrates that production of D-2HG is coupled to oxidation of 3HP in the propionate shunt. We therefore conclude that DHGD-1 functions in the propionate shunt, and that its dysfunction leads to impaired flux through this pathway, resulting in accumulation of shunt intermediates 3HP and 2HG.

Since *dhgd-1* functions in the propionate shunt, we next asked whether reducing the activity of this pathway could rescue the lethality of Δ*dhgd-1* mutants. Vitamin B12 enables flux through the canonical propionate degradation pathway and transcriptionally represses the propionate shunt[7,16,17] and supplementation of vitamin B12 fully rescued lethality in Δ*dhgd-1* mutants (Fig. 3a). Next, we asked whether inhibiting the reaction that produces D-2HG would rescue lethality in Δ*dhgd-1* mutant animals as well and indeed found that RNAi of *hphd-1* also fully rescued (Fig. 3b). What are the metabolic changes that elicit lethality in Δ*dhgd-1* mutant animals? We found that 3HP levels remain high in Δ*dhgd-1* mutants exposed to *hphd-1* knockdown (Fig. 3c). This is because both *dhgd-1* mutation and *hphd-1* RNAi likely block HPHD-1 function (Fig. 3d). Therefore, 3HP accumulation does not explain lethality of Δ*dhgd-1* mutants. However, upon *hphd-1* RNAi, D-2HG levels are dramatically reduced, because 3HP oxidation is blocked (Fig. 3e, f). This observation indicates that 3HP oxidation by HPHD-1 is the main source of D-2HG. Surprisingly, however, while 3HP levels go down in Δ*dhgd-1* mutants upon supplementation of vitamin B12, 2HG levels remain high (Figs. 3g,h). Since HPHD-1 is the primary source of D-2HG, this observation suggests that there is still flux through the propionate shunt pathway in Δ*dhgd-1* mutant animals supplemented with vitamin B12. Altogether, we conclude that the embryonic lethal phenotype in Δ*dhgd-1* mutants is caused neither exclusively by high levels of 3HP nor by high levels of 2HG. Finally, vitamin B12 supplementation, but not *hphd-1* RNAi, rescued the mitochondrial defects of Δ*dhgd-1* mutants (Extended Data Figure 1a,b). Thus, high 3HP levels correlate with mitochondrial defects, which is consistent with a recent study[13]. Importantly, this result demonstrates

that mitochondrial defects are not sufficient to cause lethality and, therefore, that these two phenotypes of Δ*dhgd-1* mutants are caused, at least in part, by distinct mechanisms.

To gain insight into the mechanism by which loss of *dhgd-1* causes embryonic lethality we used expression profiling by RNA sequencing (RNA-seq). Overall, we found that 315 and 183 genes are induced and repressed by loss of *dhgd-1*, respectively (Extended Data Table 2). WormFlux[18] pathway enrichment analysis using pathways defined by WormPaths[19] showed that the propionate shunt is not fully repressed by vitamin B12 in Δ*dhgd-1* mutants (Figs. 4a, b, Extended Data Table 3). This observation indicates that the propionate shunt remains somewhat active and can explain why 2HG levels remain high in these animals, even in the presence of vitamin B12 (Fig. 3h). Interestingly, the RNA-seq data revealed an upregulation of ketone body metabolism genes in Δ*dhgd-1* mutants, both in the presence and absence of vitamin B12 supplementation, as well as downregulation of these genes in wild type animals supplemented by vitamin B12 (Figs 4a, b).

We next asked if perturbed ketone body metabolism in Δ*dhgd-1* mutant animals could be causing embryonic lethality. In *C. elegans*, as in humans, there are two strictly ketogenic amino acids: leucine and lysine. Our metabolomic data showed that the breakdown of these amino acids is impaired in Δ*dhgd-1* mutants: lysine levels are increased while its breakdown products 2-aminoadipate and glutarate are decreased, and the leucine breakdown product HMB is increased (Fig. 2a and Extended Data Fig. 3). Another key precursor for ketone body production is acetyl-CoA, which is the product of the propionate shunt pathway, and flux through this pathway is also impaired in Δ*dhgd-1* mutants (Fig. 2c,d)[7]. In humans, ketone bodies are energy substrates when glucose is limited. Therefore, we hypothesized that lack of ketone body and/or energy production may contribute to embryonic lethality in Δ*dhgd-1* mutant animals. We first performed flux balance analysis (FBA) with the genome-scale *C. elegans* metabolic network model iCEL1314 we previously reconstructed[18,20]. FBA predicted that combined loss of flux through the propionate shunt and lysine and leucine degradation pathways greatly reduces ketone body and energy production, which provides support for our hypothesis (Fig. 4c). Next, we tested our hypothesis more directly by supplementing Δ*dhgd-1* mutants with 3-hydroxybutyrate

(3HB) and found that this ketone body partially rescued embryonic lethality (Fig. 4d). Since RNAi of *hphd-1* blocks flux through the propionate shunt and rescues lethality in Δ*dhgd-1* mutants (Fig. 3b), this phenotype is not simply caused by a lack of acetyl-CoA production by the propionate shunt. Rather, Δ*dhgd-1* mutant lethality may result from a ketone body deficit in two ways: a reduction in the production of the ketone body precursor acetyl-CoA by the propionate shunt, and an impairment of lysine and leucine breakdown, potentially by high levels of 2HG (Fig. 4e).

What is the physiological role of upregulating ketone body metabolism genes on low vitamin B12 diets and in Δ*dhgd-1* mutant animals? In humans, ketone bodies are synthesized by the tissues with excess acetyl-CoA (liver) and transported to tissues with high energetic demands (brain and muscle)[21]. We hypothesized that, as in humans, ketone bodies provide energy for particular tissues in *C. elegans*. For example, ketone bodies may provide energy to body wall muscles to support movement and development. By examining tissue-level single cell RNA-seq data of early larvae[22] and embryos[23], we found that expression of the genes comprising the canonical, vitamin B12-dependent propionate breakdown pathway is very high in body wall muscle (Fig. 5a, Extended Data Figure 4). This indicates that, when vitamin B12 is readily available, this pathway can be used by this tissue to produce succinyl-CoA, which can anaplerotically enter the TCA cycle to produce energy. Strikingly, expression of the first gene of the propionate shunt, *acdh-1*, is specific to the intestine and hypodermis. In *C. elegans*, these tissues function as both gut and liver, which are the primary sites of nutrient absorption, digestion, and metabolism[20,24]. The other propionate shunt genes exhibit less stringent tissue-specific expression and have been annotated to be involved in other metabolic pathways, including ketone body metabolism[19]. Since *acdh-1* expression is required for propionate shunt flux[7], this indicates that this pathway is not operational in body wall muscle early in development. Therefore, we hypothesized that, on low-vitamin B12 diets, the propionate shunt produces acetyl-CoA in the intestine (and to a lesser extent hypodermis) and that this acetyl-CoA is converted to ketone bodies, as suggested by the upregulation of ketone body metabolism genes on low-vitamin B12 diets (Fig. 4a, b). These ketone bodies can then diffuse to the body wall muscle where they are converted back to acetyl-CoA and

oxidized via the TCA cycle to produce energy (Fig. 5b). It is not feasible to directly test this hypothesis in *C. elegans* because different tissues cannot be isolated for metabolomic analyses. Therefore, we analyzed the production and consumption potential of ketone bodies, which we previously calculated using flux potential analysis[20], and found that the intestine is the greatest producer of ketone bodies, and that body wall muscle is the greatest consumer.

Taken together our data suggest that ketone bodies are essential for *C. elegans* on diets low in vitamin B12. Mutations in Δ*dhgd-1* result in insufficient generation of both ketone bodies (via breakdown of lysine and leucine) and acetyl-CoA (via the propionate shunt), thereby leading to embryonic lethality. There are different mechanisms by which embryonic lethality in Δ*dhgd-1* animals can be rescued: by direct supplementation of the ketone body 3HB, which can be converted to acetyl-CoA to produce energy; by knocking down *hphd-1*, which prevents 2HG accumulation that may inhibit the generation of ketone bodies by lysine and leucine degradation; and by supplementing vitamin B12, which facilitates production of propionate-derived succinyl-CoA in the muscle and circumvents the need for ketogenesis. Altogether, these results indicate that *C. elegans* may rely on amino acids and propionate degradation as a source of energy, and that on diets low in vitamin B12, the propionate shunt is an important producer of the ketone body precursor, acetyl-CoA. We have previously shown that the propionate shunt plays an important role in the detoxification of propionate, high levels of which are detrimental to *C. elegans*, as they are in humans[7,17]. Therefore, the results presented here indicate that the propionate shunt serves an important dual purpose: the detoxification of excess propionate, and the production of acetyl-CoA and energy.

## References


1 Struys, E. A. *et al.* Mutations in the D-2-hydroxyglutarate dehydrogenase gene cause D-2-hydroxyglutaric aciduria. *Am J Hum Genet* **76**, 358-360, doi:10.1086/427890 (2005).

2 Xu, W. *et al.* Oncometabolite 2-hydroxyglutarate is a competitive inhibitor of alpha-ketoglutarate-dependent dioxygenases. *Cancer cell* **19**, 17-30, doi:10.1016/j.ccr.2010.12.014 (2011).

3 Qing, Y. *et al.* R-2-hydroxyglutarate attenuates aerobic glycolysis in leukemia by targeting the FTO/m(6)A/PFKP/LDHB axis. *Mol Cell* **81**, 922-939 e929, doi:10.1016/j.molcel.2020.12.026 (2021).

4 Fu, X. *et al.* 2-Hydroxyglutarate Inhibits ATP Synthase and mTOR Signaling. *Cell Metab* **22**, 508-515, doi:10.1016/j.cmet.2015.06.009 (2015).

5 Losman, J. A. *et al.* (R)-2-hydroxyglutarate is sufficient to promote leukemogenesis and its effects are reversible. *Science* **339**, 1621-1625, doi:10.1126/science.1231677 (2013).
6 Colvin, H. *et al.* Oncometabolite D-2-Hydroxyglurate Directly Induces Epithelial-Mesenchymal Transition and is Associated with Distant Metastasis in Colorectal Cancer. *Sci Rep* **6**, 36289, doi:10.1038/srep36289 (2016).
7 Watson, E. *et al.* Metabolic network rewiring of propionate flux compensates vitamin B12 deficiency in *C. elegans. Elife* **5**, pii: e17670 (2016).
8 Faiyaz-Ul-Haque, M. *et al.* Clinical, neuroimaging, and genetic features of L-2-hydroxyglutaric aciduria in Arab kindreds. *Ann Saudi Med* **34**, 107-114, doi:10.5144/0256-4947.2014.107 (2014).
9 Veiga-da-Cunha, M., Van Schaftingen, E. & Bommer, G. T. Inborn errors of metabolite repair. *J Inherit Metab Dis* **43**, 14-24, doi:10.1002/jimd.12187 (2020).
10 Kranendijk, M., Struys, E. A., Salomons, G. S., Van der Knaap, M. S. & Jakobs, C. Progress in understanding 2-hydroxyglutaric acidurias. *J Inherit Metab Dis* **35**, 571-587, doi:10.1007/s10545-012-9462-5 (2012).
11 Li, H. *et al. Drosophila* larvae synthesize the putative oncometabolite L-2-hydroxyglutarate during normal developmental growth. *Proc Natl Acad Sci U S A* **114**, 1353-1358, doi:10.1073/pnas.1614102114 (2017).
12 Yang, J., Zhu, H., Zhang, T. & Ding, J. Structure, substrate specificity, and catalytic mechanism of human D-2-HGDH and insights into pathogenicity of disease-associated mutations. *Cell Discov* **7**, 3, doi:10.1038/s41421-020-00227-0 (2021).
13 Zhou, J. *et al.* A feedback loop engaging propionate catabolism intermediates controls mitochondrial morphology. *Nat Cell Biol* **24**, 526-537, doi:10.1038/s41556-022-00883-2 (2022).
14 Struys, E. A. *et al.* Kinetic characterization of human hydroxyacid-oxoacid transhydrogenase: relevance to D-2-hydroxyglutaric and gamma-hydroxybutyric acidurias. *J Inherit Metab Dis* **28**, 921-930, doi:10.1007/s10545-005-0114-x (2005).
15 Gaona-Lopez, C., Julian-Sanchez, A. & Riveros-Rosas, H. Diversity and Evolutionary Analysis of Iron-Containing (Type-III) Alcohol Dehydrogenases in Eukaryotes. *PLoS One* **11**, e0166851, doi:10.1371/journal.pone.0166851 (2016).
16 Watson, E. *et al.* Interspecies systems biology uncovers metabolites affecting *C. elegans* gene expression and life history traits. *Cell* **156**, 759-770 (2014).
17 Bulcha, J. T. *et al.* A persistence detector for metabolic network rewiring in an animal. *Cell Rep* **26**, 460-468 (2019).
18 Yilmaz, L. S. & Walhout, A. J. A *Caenorhabditis elegans g*enome-scale metabolic network model. *Cell Syst* **2**, 297-311, doi:10.1016/j.cels.2016.04.012 (2016).
19 Walker, M. D. *et al.* WormPaths: *Caenorhabditis elegans* metabolic pathway annotation and visualization. *Genetics* **219**, doi:10.1093/genetics/iyab089 (2021).
20 Yilmaz, L. S. *et al.* Modeling tissue-relevant *Caenorhabditis elegans* metabolism at network, pathway, reaction, and metabolite levels. *Mol Syst Biol* **16**, e9649, doi:10.15252/msb.20209649 (2020).
21 Puchalska, P. & Crawford, P. A. Multi-dimensional Roles of Ketone Bodies in Fuel Metabolism, Signaling, and Therapeutics. *Cell Metab* **25**, 262-284, doi:10.1016/j.cmet.2016.12.022 (2017).
22 Cao, J. *et al.* Comprehensive single-cell transcriptional profiling of a multicellular organism. *Science* **357**, 661-667, doi:10.1126/science.aam8940 (2017).
23 Warner, A. D., Gevirtzman, L., Hillier, L. W., Ewing, B. & Waterston, R. H. The *C. elegans* embryonic transcriptome with tissue, time, and alternative splicing resolution. *Genome Res* **29**, 1036-1045, doi:10.1101/gr.243394.118 (2019).
24 Kaletsky, R. *et al.* Transcriptome analysis of adult *Caenorhabditis elegans* cells reveals tissue-specific gene and isoform expression. *PLoS Genet* **14**, e1007559, doi:10.1371/journal.pgen.1007559 (2018).
25 Mitani, S. Nematode, an experimental animal in the national BioResource project. *Exp Anim* **58**, 351-356, doi:10.1538/expanim.58.351 (2009).
26 Xiao, R. *et al.* RNAi interrogation of dietary modulation of development, metabolism, behavior, and aging in *C. elegans*. *Cell Rep* **11**, 1123-1133, doi:10.1016/j.celrep.2015.04.024 (2015).
27 Hibshman, J. D., Webster, A. K. & Baugh, L. R. Liquid-culture protocols for synchronous starvation, growth, dauer formation, and dietary restriction of *Caenorhabditis elegans*. *STAR Protoc* **2**, 100276, doi:10.1016/j.xpro.2020.100276 (2021).
28 Li, H. & Tennessen, J. M. Quantification of D- and L-2-Hydroxyglutarate in *Drosophila melanogaster* Tissue Samples Using Gas Chromatography-Mass Spectrometry. *Methods Mol Biol* **1978**, 155-165, doi:10.1007/978-1-4939-9236-2_10 (2019).
29 Subramanian, A. *et al.* Gene set enrichment analysis: a knowledge-based approach for interpreting genome-wide expression profiles. *Proc Natl Acad Sci U S A* **102**, 15545-15550, doi:10.1073/pnas.0506580102 (2005).
30 Giese, G. E. *et al. Caenorhabditis elegans* methionine/S-adenosylmethionine cycle activity is sensed and adjusted by a nuclear hormone receptor. *Elife* **9**, doi:10.7554/eLife.60259 (2020).
31 Hashimshony, T. *et al.* CEL-Seq2: sensitive highly-multiplexed single-cell RNA-Seq. *Genome Biol* **17**, 77, doi:10.1186/s13059-016-0938-8 (2016).
32 Derr, A. *et al.* End Sequence Analysis Toolkit (ESAT) expands the extractable information from single-cell RNA-seq data. *Genome Res* **26**, 1397-1410, doi:10.1101/gr.207902.116 (2016).

33 Love, M. I., Huber, W. & Anders, S. Moderated estimation of fold change and dispersion for RNA-seq data with DESeq2. *Genome Biol* **15**, 550, doi:10.1186/s13059-014-0550-8 (2014).

## Online content

## Methods

***C. elegans* and *E. coli* strains.** For maintenance, *C. elegans* strains were grown on nematode growth medium (NGM) seeded with *E. coli* OP50 and supplemented with 64 nM adenosylcobalamin (vitamin B12). Experimental plates contained vitamin B12 if specified. The mutant strain F54D5.12*(tm6671)* was provided by the National Bioresource Project for Nematode *C. elegans*[25] and was backcrossed three times to N2. We named F54D5.12 *dhgd-1* for D-2-Hydroxyglutarate dehydrogenase. Wild type N2 *C. elegans* and bacterial strains *E. coli* OP50 and *E. coli* HT115 were obtained from the Caenorhabditis Genetics Center. The RNAi-compatible *E. coli* OP50(xu363) was provided by the Xu lab[26].

**Metabolite extractions.** *C. elegans* cultures maintained on *E. coli* OP50 diet supplemented with 64 nM vitamin B12 were synchronized using sodium-hydroxide-buffered sodium hypochlorite treatment. L1 larvae were plated onto NGM agar plates for specified treatment (*e.g.*, vitamin B12 supplementation, RNAi) and harvested as 1-day-old gravid adults. Animals used for experiments described in Fig. 1c were cultured in liquid S-medium[27] in conditions described in the isotope tracing section of the methods. First day gravid adults were washed three times with M9 buffer and 50 ul of the packed animal pellet was flash-frozen in a dry ice/ethanol bath and stored at -80°C. Next, samples were mixed with 1 mL 80% methanol and 0.5 mL of 200- to 300-μm acid-washed glass beads (MilliporeSigma) and homogenized using a FastPrep-24 bead beater (MP Biomedicals), with intermittent cooling in dry ice/ethanol bath. Samples were then extracted for 15 min, then centrifuged for 10 min at 20,000 × *g*, and the supernatant was used immediately or stored at -80°C.

**Targeted quantification of metabolites using gas chromatography-mass spectrometry (GC-MS).** 250 ul of animal extracts were dried under vacuum using a SpeedVac concentrator SPD111V (Thermo Fisher Scientific). Derivatization of dried samples was performed by adding 20 ul pyridine and 50 µL *N*-methyl-*N*-(trimethylsilyl)trifluoroacetamide (MSTFA, MilliporeSigma) and incubating samples for three hours at 37° C, followed by five hours incubation at room temperature. In the experiments that also targeted αKG, dried samples received 20 µL of 20 mg/mL methoxyamine hydrochloride in pyridine (MilliporeSigma) and were incubated at 37° C for one hour before reaction with MSTFA derivatization. Measurements were performed on an Agilent 7890B single quadrupole mass spectrometry coupled to an Agilent 5977B gas chromatograph (GC-MS) with an HP-5MS Ultra Inert capillary column (30 m × 0.25 mm × 0.25 µm). The inlet temperature was set to 230°C, the transfer line was at 280°C, and the MS source and quadrupole were at 230°C and 150°C, respectively. The oven was programmed to start at 80°C, hold for 2 min, and ramp-up at 5°C/min until 280°C. Each metabolite was identified based on retention time, one quantifier, and two qualifier ions that were manually selected using a reference compound. Peak integration and quantification of peak areas was done using MassHunter software, blank subtraction and normalization to total quantified metabolites were done in R software.

**Relative quantification of D- and L-2HG.** To distinguish the two enantiomers of 2HG we adapted a previously published protocol[28]. First, 300 ul of *C. elegans* metabolite extract was evaporated to dryness in glass inserts. 50 ul of R-(-)-butanol and five ul of 12N hydrochloric acid were added to each insert and incubated at 90°C with shaking for three hours. Samples were cooled to room temperature and transferred into glass tubes containing 400 ul hexane. After extraction 250 ul of organic phase were transferred into a new glass insert and evaporated to dryness. Next, 30 ul of pyridine and 30 ul of acetic anhydride were added to each sample and allowed to incubate for one hour at 80°C with shaking. Samples were dried, resuspended in 60 ul of hexane, and immediately analyzed by GC-MS using targeted method settings, with exception of oven ramp, which was run from 80 to 190°C at the rate of

5°C/min and then until 280°C at 15°C/min. 173 m/z ion was used for quantification of both D- and L-2HG.

**Brood size and hatching assays.** Seven L4-stage animals per strain/condition were placed on individual 3.5 cm plates and transferred to a new plate every 24 hours until animals stopped laying eggs. Plates with embryos were incubated for 24 hours and then the number of hatched L1 larvae and unhatched embryos were counted and averaged for all animals. Brood counts for animals that died or crawled off the plate before egg-laying was complete were excluded. The experiment was repeated three times.

**Mitochondrial network imaging.** Wild type and Δ*dhgd-1 C. elegans* strains were crossed to a strain with fluorescently labeled mitochondria and nuclei *Pmyo-3::GFP*mito; *Pmyo-3::lacZ::GFP*(nls) in body wall muscles. At least 10 L4 animals per condition were imaged using Nikon A1 point-scanning confocal microscope with 561 nm laser. Imaging was performed using an Apo TIRF, N.A. 1.49, 60x oil immersion objective in galvano imaging mode.

**Gene coexpression analysis.** A ranked list of metabolic genes that are coexpressed with *dhgd-1* was extracted from a compendium of 169 expression datasets. Briefly, z-normalized expression datasets with at least 10 conditions were combined to form a global coexpression matrix. Correlation in expression between metabolic gene pairs across the compendium was calculated as Pearson Correlation Coefficient. Gene set enrichment analysis (GSEA) was performed on the ranked coexpression list using the PreRank module of GSEA[29] with pathway-to-gene annotations from WormPaths[19] and the significance cutoff set at a FDR of less than or equal to 0.05.

**Deuterium isotope tracing.** Gravid adults were treated with sodium-hydroxide-buffered sodium hypochlorite solution to obtain synchronous L1 populations. Approximately 50,000 L1 animals were

added per 50 ml Erlenmeyer flask containing 10 ml of K-medium with modified salt concentrations (51 mM NaCl, 32 mM KCl, 3 mM CaCl2, 3 mM MgSO4) and *E. coli* OP50 pellet from a 100 ml of overnight culture. Cultures were incubated at 20°C with shaking at 180 rpm. Propionic acid (MilliporeSigma) or $^{2}H_{5}$-propionic acid (Cambridge Isotope Laboratories), neutralized with sodium hydroxide, were added to the cultures when animals reached the late L4/young adult stage to a final concentration of 20 mM. *C. elegans* were harvested at the gravid adult stage (about 12 h after supplementation), washed three times, flash-frozen in ethanol/dry ice bath, and stored at -80°C. Metabolite extraction, derivatization, and GC-MS methods were as described above. M+0 3HP and 2HG were quantified as *m/z* 219 and *m/z* 247, respectively. Relative isotopic enrichment was calculated as $\frac{R}{R+1} \times 100$, where R is a difference between abundances (normalized to the M+0 ion) of isotopologues in a sample with labeled propionate and a sample with unlabeled propionate supplement.

**HPLC-MS analysis.** Reversed-phase chromatography was performed using a Vanquish HPLC system controlled by Chromeleon Software (ThermoFisher Scientific) and coupled to an Orbitrap Q-Exactive HF mass spectrometer controlled by Xcalibur software (ThermoFisher Scientific). Extracts prepared as described above were separated on a Thermo Scientific Hypersil Gold column (150 mm x 2.1 mm, particle size 1.9 µm) maintained at 40 °C with a flow rate of 0.5 mL/min. Solvent A: 0.1% formic acid in water; solvent B: 0.1% formic acid in acetonitrile. A/B gradient started at 1% B for 3 min after injection and increased linearly to 98% B at 20 min, followed by 5 min at 98% B, then back to 1% B over 0.1 min and finally held at 1% B for an additional 2.9 min to re-equilibrate the column. Mass spectrometer parameters: spray voltage (-3.0 kV, +3.5 kV), capillary temperature 380 °C, probe heater temperature 400 °C; sheath, auxiliary, and sweep gas 60, 20, and 2 AU, respectively. S-Lens RF level: 50, resolution 120,000 at m/z 200, AGC target 3E6. Samples were injected and analyzed in negative and positive electrospray ionization modes with m/z range 117-1000. Analysis was performed with Xcalibur QualBrowser v4.1.31.9 (Thermo Scientific).

**Metabolite supplementation.** For experiments using vitamin B12 supplementation, NGM agar plates were supplemented with 64 nM adenosylcobalamin before pouring plates. DL-3-hydroxybutyric acid sodium salt (MilliporeSigma) was supplemented in indicated concentrations to NGM agar media.

**Embryonic lethality assays.** Gravid adults were treated with sodium-hydroxide-buffered sodium hypochlorite solution, and released embryos were washed and incubated in M9 buffer for 18 hours to obtain synchronized L1 animals. Approximately 30 animals were placed onto 3.5 cm NGM plates (seeded with 100 ul of overnight bacterial culture one day before) and allowed to lay eggs. Adult animals were washed away with M9 buffer and approximately 200-300 embryos were transferred onto a new plate with the same supplements. After 24 hours hatched and not hatched animals were counted.

**RNAi assays.** RNAi experiments were done using *E. coli* OP50(xu363) [26] transformed with either empty vector L4440 or RNAi plasmid. Bacterial cultures were grown 18-20 hours and seeded onto NGM agar plates containing 2 mM isopropyl β-D-1-thiogalactopyranoside (IPTG), 50 µg/mL ampicillin, and used for metabolomics or phenotypic assays as described.

**Expression profiling by RNA-seq.** 200-300 synchronized gravid adults were harvested from *E. coli* OP50-seeded NGM plates with or without supplemented 64 nM adenosylcobalamin. Animals were washed three times with M9 buffer and total RNA from their bodies (excluding embryos) was extracted using the RNeasy kit (Qiagen), with an additional step of on-column DNase I (NEB) treatment. RNA quality was verified by agarose gel electrophoresis.

RNA-sequencing was performed as previously described[30]. Briefly, multiplexed libraries were prepared using Cel-seq2[31]. Two biological replicates were sequenced with a NextSeq 500/550 High Output Kit v2.5 on a Nextseq500 sequencer and three other replicates were sequenced on MGISEQ-2000. The libraries were first demultiplexed by a homemade python script, and adapter sequences were trimmed using trimmomatic-0.32 by recognizing polyA and barcode sequences. Then, the

alignment to the reference genome was performed by STAR. Features were counted by ESAT[32] with pseudogenes discarded. The read counts for each gene were used in differential expression analysis by DESeq2 package in R 3.6.3[33]. Batch effects were corrected in DESeq2 statistical model by adjusting the design formula.

**Flux balance analysis.** Flux balance analysis was done using established methods [18] with the *C. elegans* metabolic network model iCEL1314[20], which can be accessed at http://wormflux.umassmed.edu/. Before simulations, the model was modified by associating HPHD-1 solely with the oxidation of 3HP[7]. In all simulations, regular model constraints, such as allowed bacterial intake and forced growth-independent maintenance energy cost, were applied using reaction boundaries. With two additional constraints, glyoxylate shunt pathway was made irreversible and propionate secretion was prevented (i.e., by setting the lower boundary of reaction RM00479 and the upper boundary of reaction EX00163 as zero, respectively). A background metabolic activity was set using reaction BIO0107, which produces biomass with all possible macro-components[20], as the objective function. The flux of this reaction was maximized first without any additional constraints. Then, to address low B12 conditions, the flux of methionine synthase (MS) reaction (RC00946) was constrained to half of its value and the maximization was repeated. This constraint reduced the biomass flux (i.e., the maximum flux of BIO0107) by about 9% as expected [18]. In subsequent simulations, the flux of BIO0107 was constrained to be at least at this level to represent the background metabolic activity. FBA results were obtained using objective functions that maximized the fluxes of reactions RCC0005, EX00164, EX03197, which represent the generation of energy, and the production of acetoacetate and 3HB, respectively. For each objective, five FBA runs were done using the following constraints in relation to the simulated perturbations: (i) no additional constraint was applied to represent wild type animals with high availability of vitamin B12; (ii) RC00946 was constrained to half of its optimal value as described above and methylmalonyl-CoA mutase reaction (RM00833) was constrained to zero value to represent low vitamin B12 conditions and the elimination of canonical

propionate breakdown; (iii) DHGD-1 reaction (RM03534) was constrained to zero flux to represent the mutated *dhgd-1* and resulting removal of flux through the propionate shunt; (iv) *aass-1*, L-lysine-alpha-ketoglutarate reductase reaction (RM00716), was constrained to zero flux to represent the lack of lysine degradation; and (v) methylcrotonoyl-CoA carboxylase reaction (RM04138) was constrained to zero flux to represent the lack of leucine degradation. The constraint of each run was added in the respective order, while maintaining the constraints from previous runs.

**Data availability**

Sequencing data have been deposited in GEO under accession code GSE201645.

**Acknowledgements**

We thank members of the Walhout lab, especially Yong-Uk Lee, for discussion and critical feedback on the manuscript.

**Author contributions**

O.P. and A.J.M.W. conceived the project. O.P. performed all experiments and analyses with help from H.Z., G.G and X.L. (RNA-seq), S.N. (gene coexpression analysis), T.L. (3-HB supplementation) and B.F. (HPLC-MS). S.L.Y. performed flux balance analysis. O.P. and A.J.M.W. wrote the paper with input from all other authors.

**Funding**

This work was supported by grants GM122502 and DK068429 from the National Institutes of Health to A.J.M.W. and DK115690 to A.J.M.W. and F.S., and by a grant from the Li Weibo Institute for Rare Disease at University of Massachusetts Chan Medical School to A.J.M.W.

**FIGURE LEGENDS**

**Fig. 1 | *dhgd-1* encodes a D-2-hydroxyglutarate (D-2HG) dehydrogenase. a**, Metabolic reaction catalyzed by D-2HG dehydrogenase. **b**, Schematic of deletion in *dhgd-1*(*tm6671*) mutants, referred to as Δ*dhgd-1* mutants. **c**, GC-MS measurement of 2HG accumulation in Δ*dhgd-1* mutants and wild type (WT) animals. Each dot represents an independent biological replicate. **d**, Discrimination between D- and L-2HG enantiomers by chiral GC-MS derivatization in WT and Δ*dhgd-1* mutant animals. Raw data are not normalized and therefore do not reflect 2HG concentration in different samples. **e,f**, Embryonic lethality and brood size in Δ*dhgd-1* mutants. Brightfield images (**e**) and hatching (**f**). Scale bar 50 um. Bars in (f) represent mean and standard deviation of n=3 biological replicates. n.s. – not significant.

**Fig. 2 | *dhgd-1* functions in the propionate shunt pathway. a**, GC-MS profiling of metabolic changes in Δ*dhgd-1* mutants compared to WT *C. elegans.* P-values are Benjamini-Hochberg adjusted. **b**, Metabolic genes most highly coexpressed with *dhgd-1*. Propionate shunt pathway genes are enriched with a false discovery rate (FDR) of 0.042 (Extended Data Table 1). **c**, **d**, Proposed mechanism of D-2HG production (by HPHD-1) and recycling (by DHGD-1) during propionate degradation via the propionate shunt pathway. **e,** Isotope tracing experiment with deuterium ($^{2}H$)-labeled propionate and proposed reaction mechanism. HPHD-1 uses $NAD^{+}$/NADH as a hydride shuttle in a coupled reaction yielding one equivalent each of MSA and D-2HG. **f**,**g,** Fractional enrichment of 3HP (**f**) and 2HG (**g**) isotopologues. Bars indicate mean of n=3 biological replicates. **h**, High performance liquid chromatography mass spectrometry (HPLC-MS) analysis of the M+1 isotope cluster in animals fed $^{2}H_{5}$-propionate revealed robust incorporation of a single deuterium atom in 2HG, whereas the M+1 in animals fed propionate was exclusively from natural abundance of $^{13}C$.

**Fig. 3 | Rescue of lethality in Δ*dhgd-1* mutants by vitamin B12 supplementation and *hpdh-1* RNAi. a,** Vitamin B12 rescues lethality in Δ*dhgd-1* mutants. Each dot represents an independent biological replicate and bars indicate means. **b,** *hphd-1* RNAi rescues lethality in Δ*dhgd-1* mutants. The RNAi-compatible *E. coli* OP50 strain[26] was used because conventional RNAi-compatible *E. coli* HT115

rescued embryonic lethality of Δ*dhgd-1* animals. Each dot represents an independent biological replicate and bars indicate means. **c,** 3HP abundance in Δ*dhgd-1* mutants upon RNAi of *hphd-1.* Boxplot midline represents median of four independent biological replicates (dots). **d,** Schematic of HPHD-1 and DHGD-1 contributions to 3HP accumulation. **e,** 2HG abundance in Δ*dhgd-1* mutants upon RNAi of *hphd-1.* Boxplot midline represents median of independent biological replicates (dots). **f,** Schematic of HPHD-1 and DHGD-1 contributions to 2HG accumulation. **g,** 3HP abundance in Δ*dhgd-1* mutants supplemented with vitamin B12. Boxplot midline represents median of independent biological replicates (dots). **h,** 2HG abundance in Δ*dhgd-1* mutants supplemented with vitamin B12. Boxplot midline represents median of independent biological replicates (dots). All panels: *p<0.05, **p<0.01, ***p<0.001 (unpaired t-test).

**Fig. 4 | Loss of *dhgd-1* activates the expression of ketone body metabolism genes.**
**a,** Gene expression pathway enrichment analysis for animals with and without vitamin B12 (B12). **b,** RNA-seq data for propionate shunt (top) and ketone body metabolism genes (bottom). TPM – transcripts per million. **c,** Contribution of propionate shunt (*dhgd-1*), lysine (*aass-1*) and leucine (*mccc-1*) degradation pathways to the generation of energy (ATP) and ketone bodies (3HB and acetoacetate). Metabolite production potentials were estimated by maximizing their output fluxes in corresponding FBA formulations. **d,** 3HB supplementation partially rescues lethality of Δ*dhgd-1* mutant animals. **e,** Model for interplay between propionate and ketone body metabolism.

**Fig. 5 | Propionate degradation in different tissues. a,** Tissue expression of genes comprising the two *C. elegans* propionate degradation pathways: the canonical, vitamin B12-dependent pathway (top) and propionate shunt (bottom) from a published single cell RNA-seq dataset[22]. **b,** Model for ketone body exchange between *C. elegans* intestine and muscle in the absence of vitamin B12.

**EXTENDED DATA FIGURE LEGENDS**

**Extended Data Fig. 1 | Mitochondrial defects in Δ*dhgd-1* mutants. a, b,** Representative images of mitochondria labelled with *Pmyo-3::GFP*mito in the wall body muscle of L4 larval stage animals. Defects in mitochondrial morphology of Δ*dhgd-1* mutant *C. elegans* is rescued by supplementing vitamin B12 (**a**) but not by *hphd-1* RNAi (**b**). Scale bar 10 um. Nuclei are marked with 'n'.

**Extended Data Fig. 2 | 3HP and 2HG measurements by GC-MS. a,b,** GC-MS quantification of 3HP (**a**) and 2HG (**b**) in *C. elegans* and *E. coli* OP50 supplemented with propionate, $^{2}H_{5}$-propionate or untreated. Bars represent mean, each dot represents an independent biological replicate,

**Extended Data Fig. 3 |.** GC-MS measurement of intermediates in degradation of ketogenic amino acids lysine and leucine. **a,b,c,** GC-MS quantification of lysine (**a**), 2-aminoadipate (**b**), HMB (**c**) and glutarate (**d**) in Δ*dhgd-1* mutants and wild type (WT) animals. Each dot represents an independent biological replicate, **$p<0.01$, ***$p<0.001$.

**Extended Data Fig. 4 |.** Embryonic tissue expression of genes comprising the two *C. elegans* propionate degradation pathways. Canonical, vitamin B12-dependent pathway (top) and propionate shunt (bottom) from a published dataset[23].

## EXTENDED DATA TABLES

**Extended Data Table 1:** Gene sets enriched in genes coexpressed with *dhgd-1*.

**Extended Data Table 2:** Genes differentially expressed in Δ*dhgd-1* mutant *C. elegans* as compared to wild type.

**Extended Data Table 3:** WormFlux pathway enrichment analysis of genes differentially expressed in Δ*dhgd-1* mutant animals with and without vitamin B12.

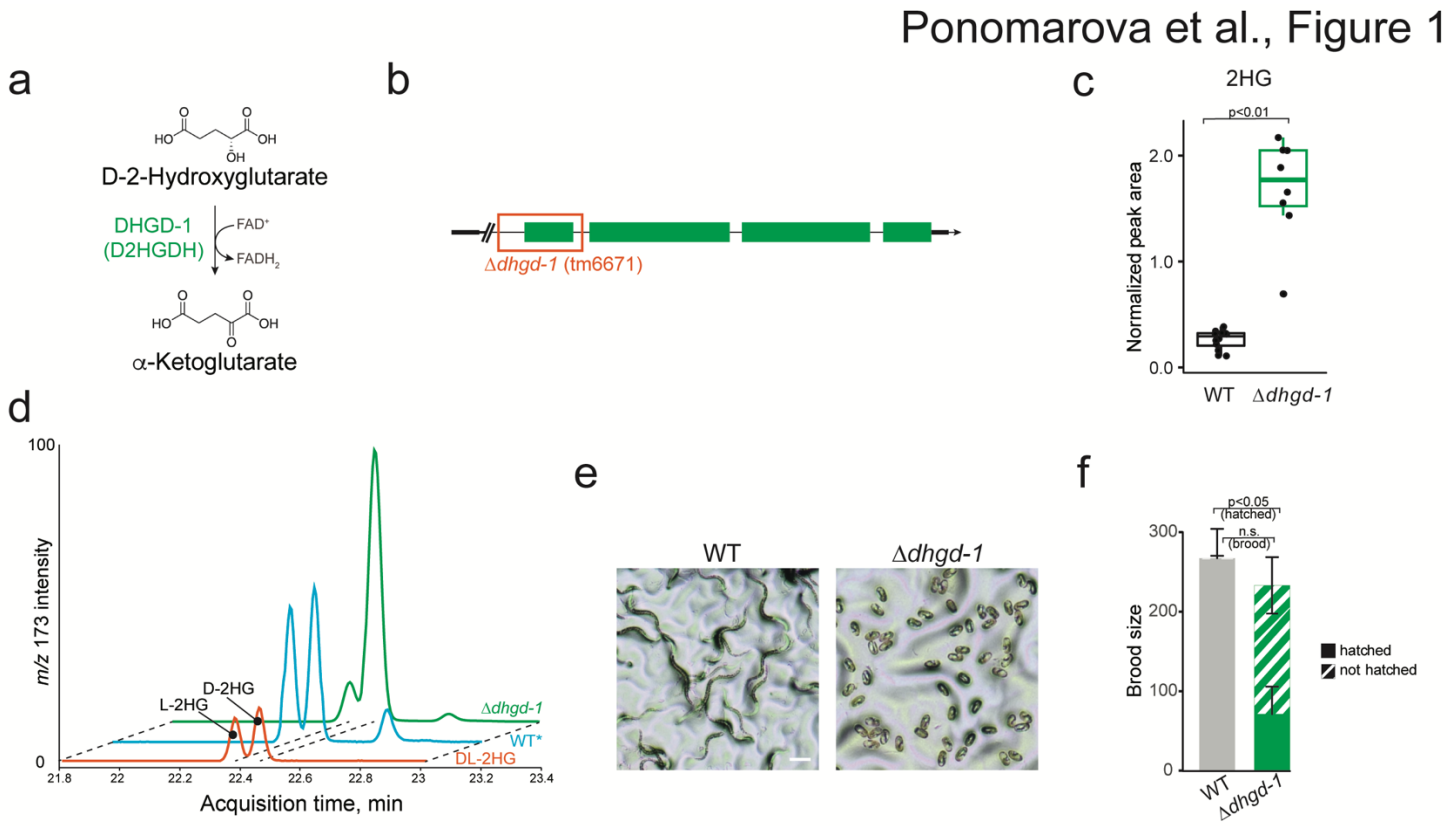

# Ponomarova et al., Figure 2

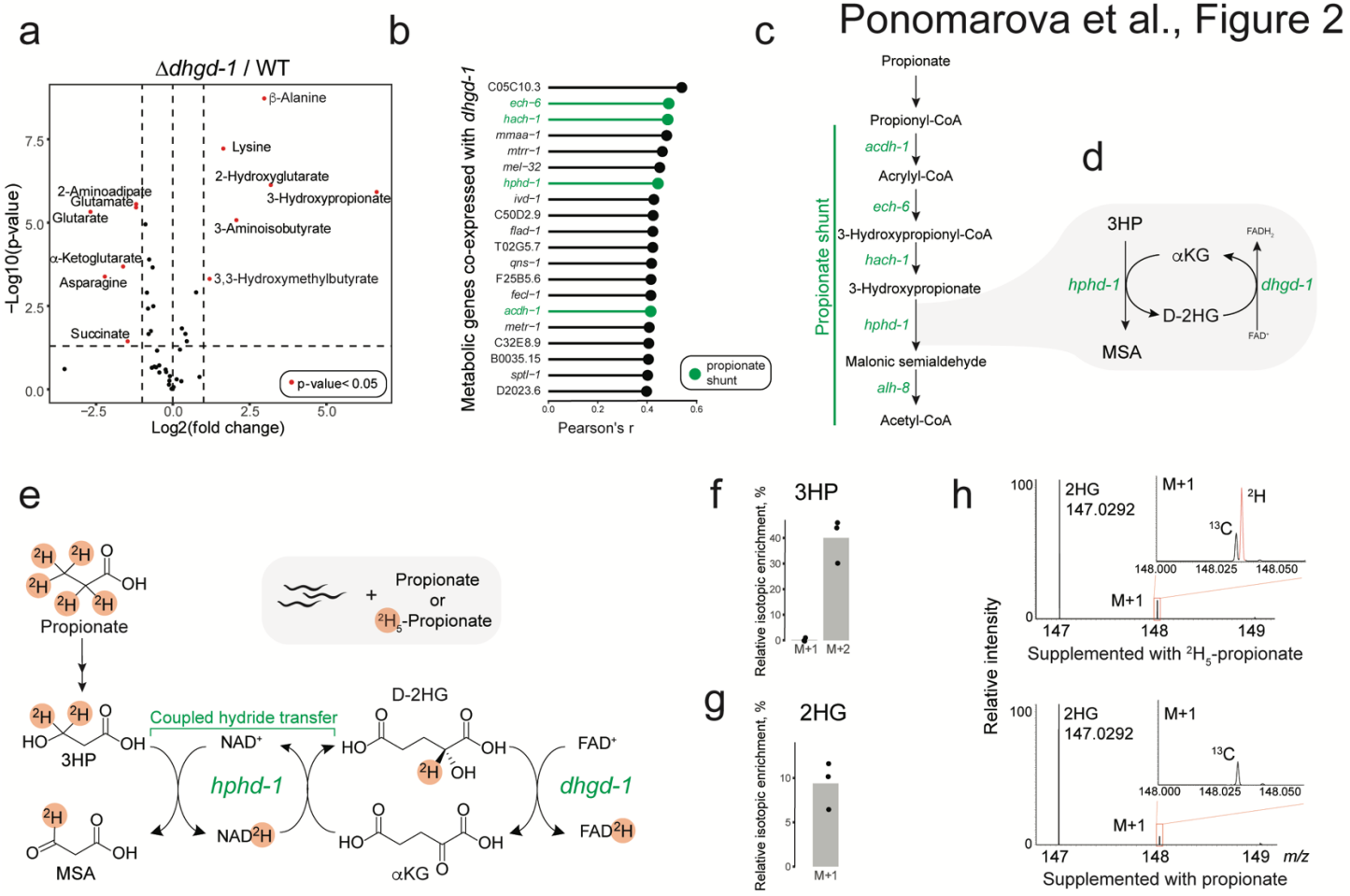

Ponomarova et al., Figure 3

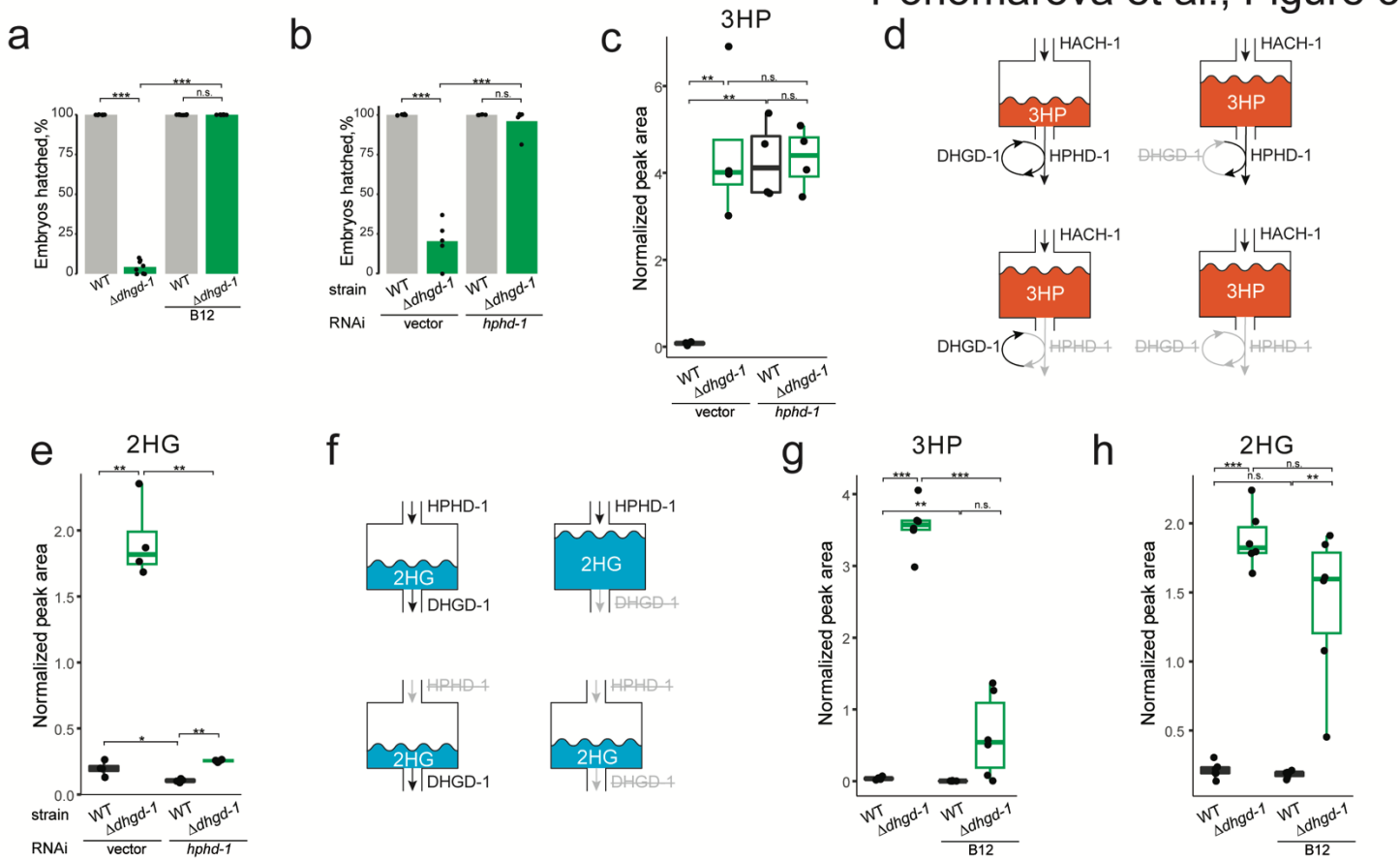

Ponomarova et al., Figure 4

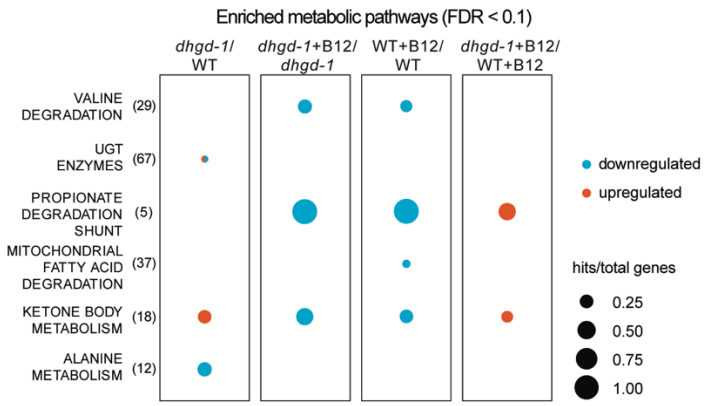


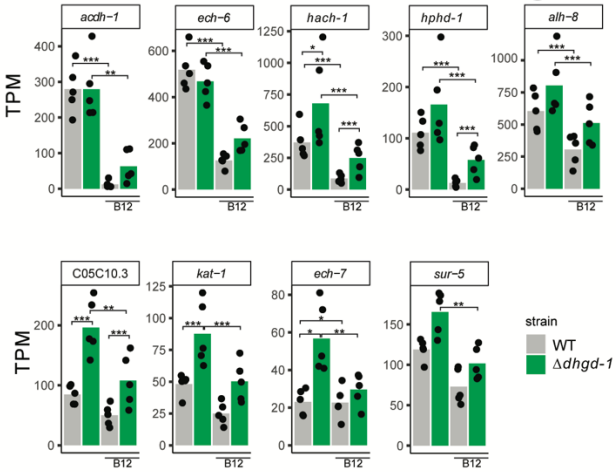


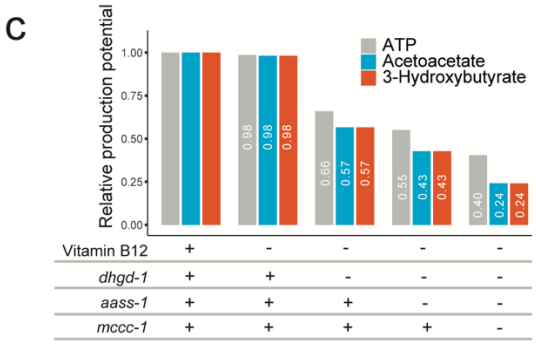


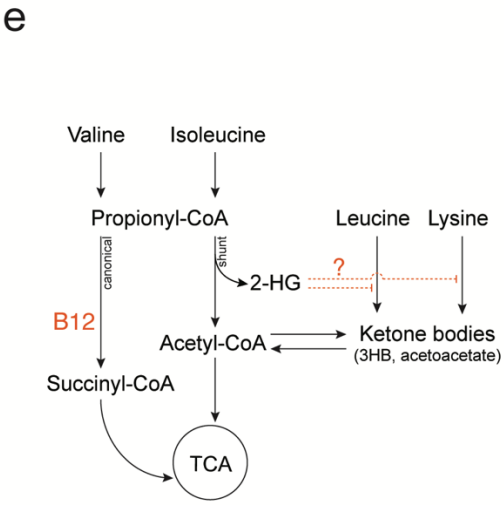


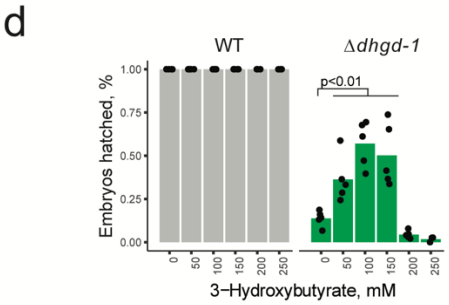

# Ponomarova et al., Figure 5

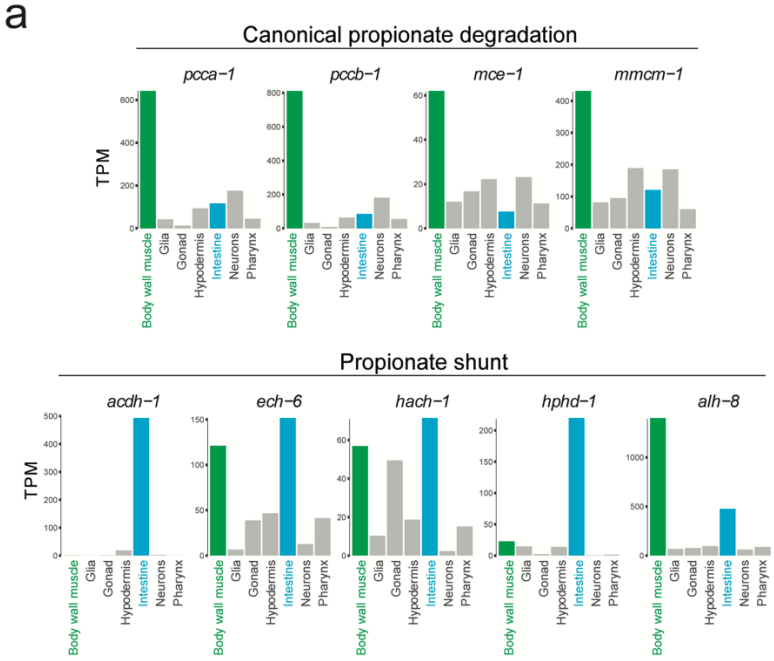


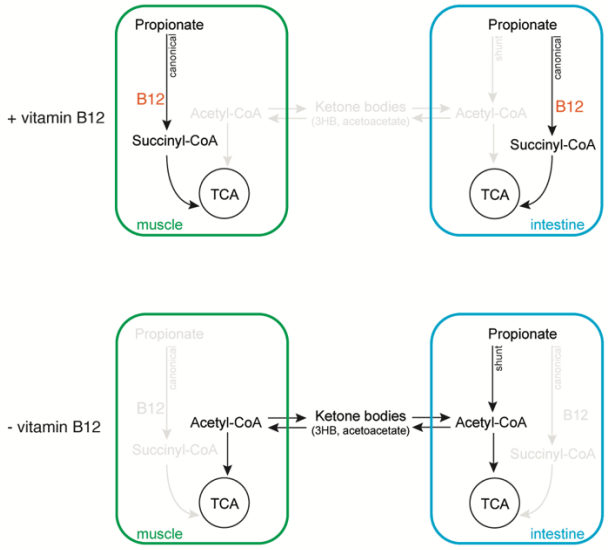

Ponomarova et al., Extended Data Figure 1

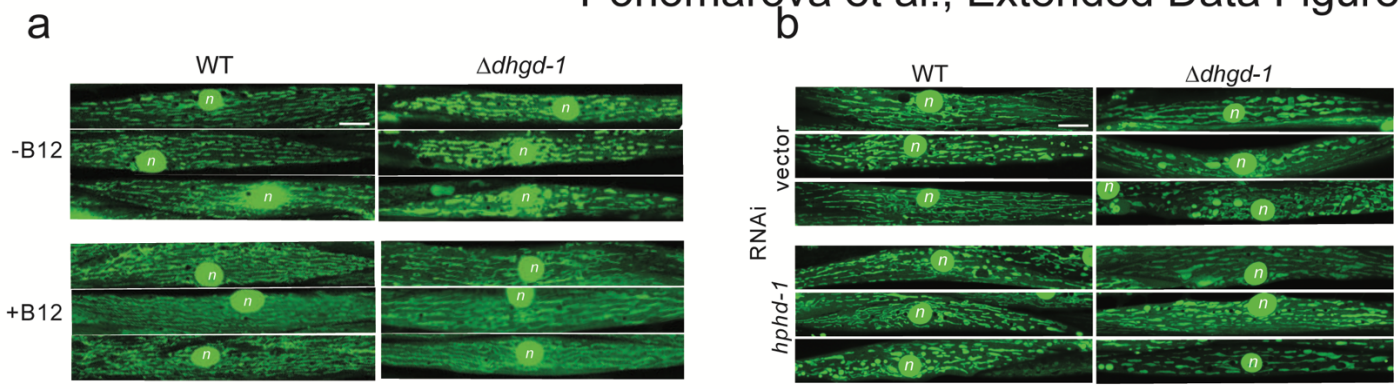

Ponomarova et al., Extended Data Figure 2

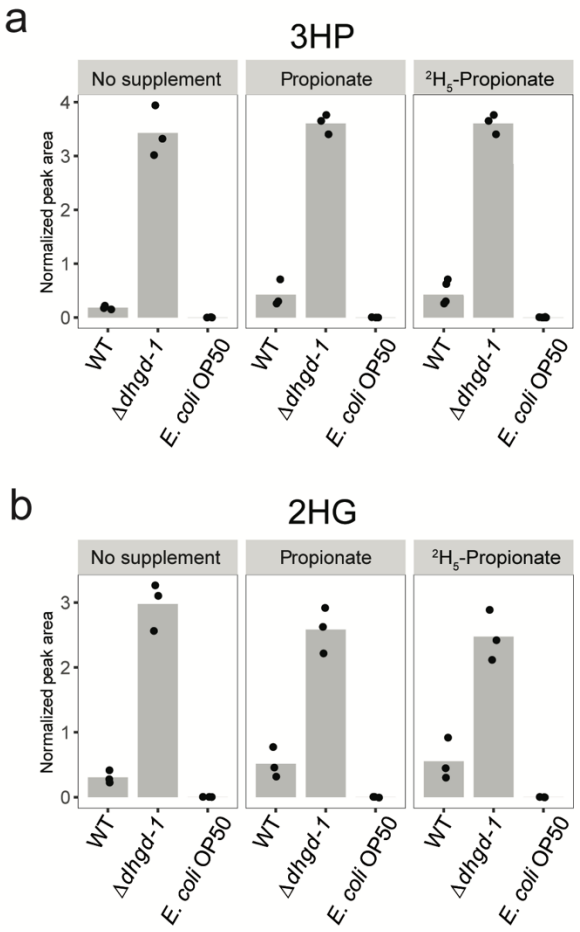

Ponomarova et al., Extended Data Figure 3

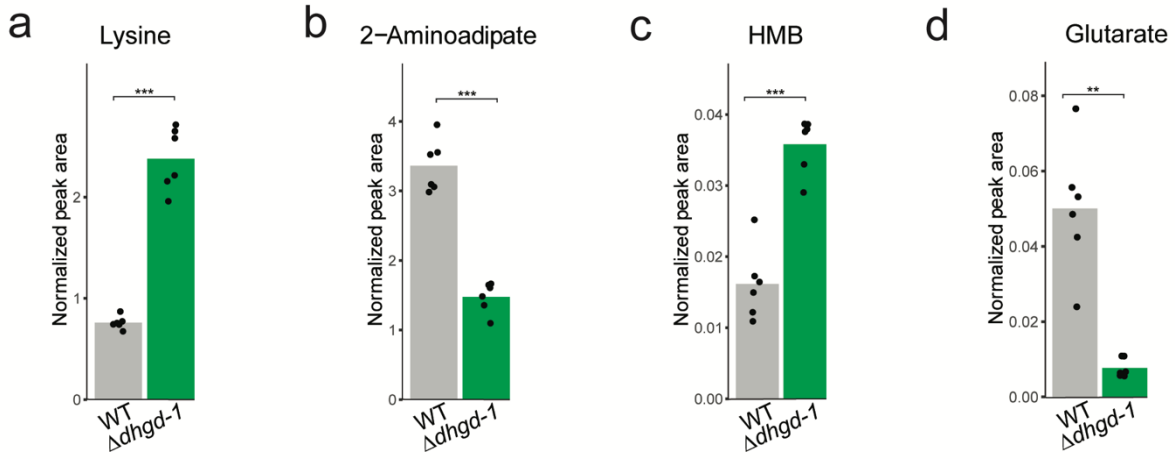
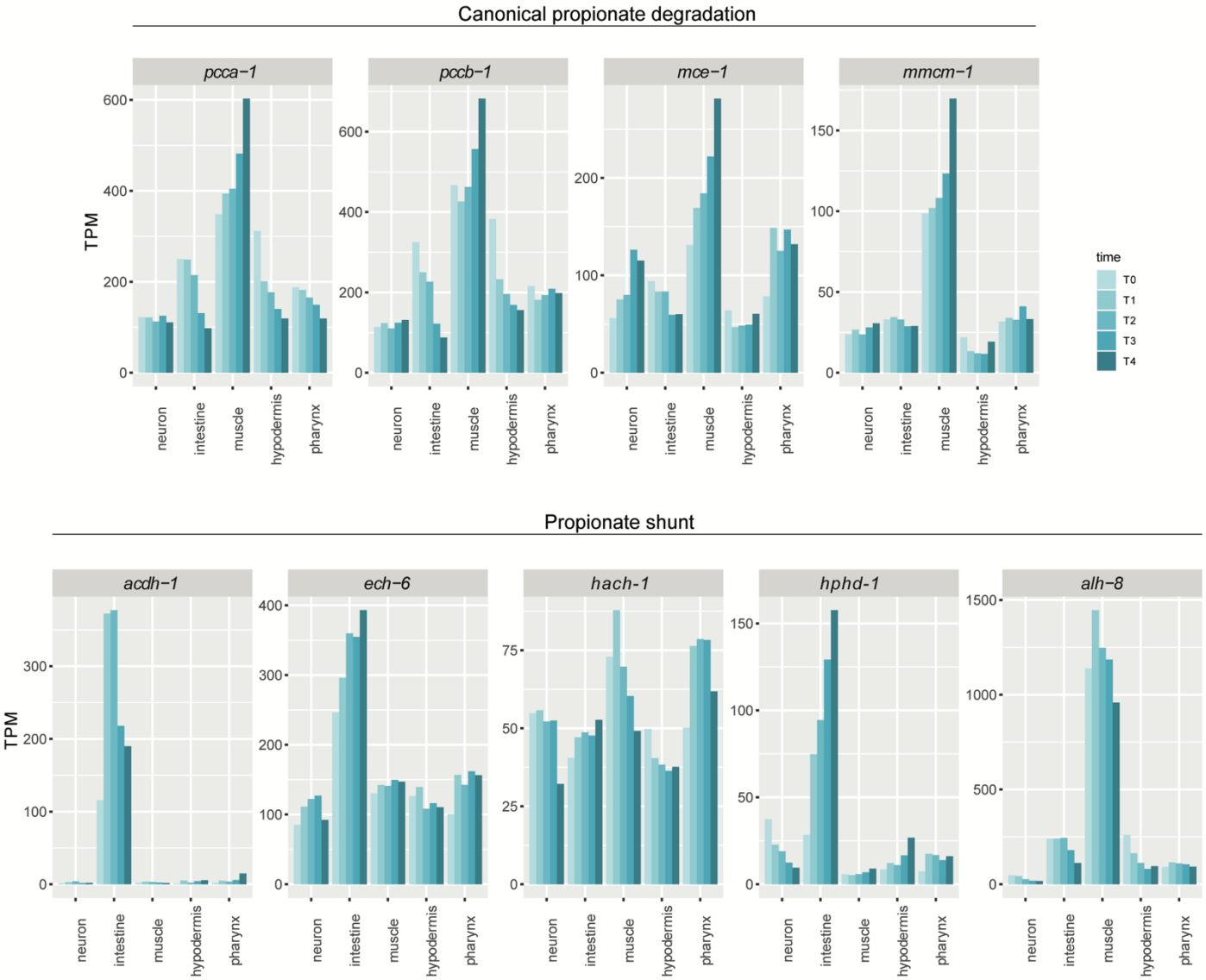
# Ponomarova et al., Extended Data Figure 4